Solar Energy
And Sustainable Development
Refereed, biannual scientific journal issued by
Center for Solar Energy Research and Studies

Environmental Stability Evaluation of Aluminium Doped Zinc Oxide (AZO) Transparent Electrodes Deposited at Low Temperature for Solar cells

S. O. Elhamali[1], M. N. Akhil[2], K. M. Abusabee[3], N. Kalfagiannis[4], and D. C. Koutsogeorgis[5]

[1,2]Electrical and Computer Engineering Department, Faculty of Engineering, Al-Alsmarya Islamic University, Zliten, Libya

[3]Electrical and Computer Engineering Department, Faculty of Engineering, El-Mergib University, Al-Khums, Libya

[4,5]School of Science and Technology, Nottingham Trent University, Clifton Lane, Nottingham NG11 8NS, UK

Email: [1*]s.elhmali@asmarya.edu.ly, [2]m.akhil@asmarya.edu.ly, [3]kmabusabee@elmergib.edu.ly, [4]Nikolaos.kalfagiannis@ntu.ac.uk, [5]Demosthenes.koutsogeorgis@ntu.ac.uk

Abstract: The degradation of transparent electrodes' electrical conductivity under environmental conditions is considered as a major failure mode for solar cells' long-term efficiency. In this paper, AZO thin films were subjected to the International Electrotechnical Commission (IEC) 61646 test to examine their environmental stability and suitability as front electrodes for solar cells. To explore the interplay between AZO deposition parameters and environmental stability, AZO films were deposited by radio frequency magnetron sputtering at different parameters and without external heating. The conductivity stability evolution upon the test was investigated via studying the AZO electrical, structural, and morphological characteristics at different deposition conditions. A direct dependence was identified between the samples' conductivity degradation rates and the samples' structural and morphological characteristics including grain size, grain boundary density, surface roughness, and compactness. The samples' resistivity increases linearly over the test period due to both electron density and mobility degradations. Improved stability was observed for thicker AZO samples (360 nm) originated from enhanced grain size, surface profile, and compactness. These samples maintained solar cells applicable sheet resistance of 21.24 Ω/sq (ρ=7.64×10^{-4} Ω.cm) following the test. The

* *Corresponding author*

DOI: 10.51646/jsesd.v11i1.122

conducted aging studies demonstrated that manipulating the AZO films' growth process via optimising the deposition parameters is an effective pathway for low temperature deposited electrodes with enhanced environmental stability.

تقييم الاستقرار البيئي للأقطاب الكهربائية الشفافة لأكسيد الزنك المطعم بالألومنيوم (AZO) المرسبة عند درجة حرارة منخفضة للخلايا الشمسية

سالم عمر الهمالي*، محمد نجيب كحيل، خيري مفتاح أبوصبيع، نيكولاوس كالفاجيانيس، و ديموستينس كوتسوجورجيس

[2,1] قسم الهندسة الكهربائية والحاسوب، كلية الهندسة، الجامعة الأسمرية الإسلامية، زليتن - ليبيا

[3] قسم الهندسة الكهربائية والحاسوب، كلية الهندسة، جامعة المرقب، الخمس - ليبيا

[5,4] مدرسة العلوم والتكنولوجيا، جامعة نوتنغهام ترينت، كليفتون لين، نوتنغهام- NG11 8NS المملكة المتحدة

ملخص: يعتبر تدهور موصلية الأقطاب الأمامية الشفافة للخلايا الشمسية تحت تأثير الظروف البيئية نمط فشل رئيسي لكفاءة الخلايا الشمسية على المدى الطويل. في هذا البحث، خضعت أفلام رقيقة من أكسيد الزنك المطعم بالألومنيوم (AZO) إلى اختبار اللجنة الكهروتقنية الدولية (IEC 61646) لاختبار استقرارها البيئي ومدى ملاءمتها كأقطاب أمامية للخلايا الشمسية. تم تصنيع أفلام (AZO) عن طريق الترسيب الفيزيائي ببلازما التردد الراديوي (Radio Frequency) دون تسخين متعمد وعند متغيرات ترسيب مختلفة لدراسة الترابط بين متغيرات الترسيب والاستقرار البيئي لأفلام (AZO). تم تحليل سلوك الموصلية الكهربائية تحت ظروف الاختبار (IEC 61646) من خلال دراسة الخصائص الكهربائية والبنيوية والمورفولوجية لأفلام (AZO) عند متغيرات الترسيب المختلفة. لوحظ وجود اعتماد مباشر بين معاملات تدهور الموصلية الكهربائية (Degradation Index) والخصائص البنيوية والمورفولوجية للعينات، بما في ذلك متوسط حجم الحبيبات وكثافة حدود الحبيبات وخشونة وتجانس سطح العينات. تعتمد هذه الخصائص على متغيرات الترسيب المستخدمة في التصنيع، ويمكن أن توفر هذه الخصائص امتصاصًا أسهل للشوائب البيئية من بيئة الاختبار الي أفلام (AZO). وبالتالي، تعمل الشوائب المتصة كمصائد للإلكترونات بين حبيبات (AZO) مما يودي الي زيادة جهد العائق (Potential Bar-rier) بين الحبيبات المتجاورة والي زيادة مقاومة العينات خطيًا خلال فترة الاختبار وذلك نتيجة لتدهور كثافة وحركة الإلكترونات. لوحظ استقرار بيئي محسّن لعينات (AZO) بسمك 360 نانومتر، تم إسناد هذا التحسن في الاستقرار البيئي الي زيادة حجم الحبيبات وتحسن نعومة وتجانس سطح العينات مع زيادة السمك. حافظت هذه العينات على مقاومة رقائق (Sheet Resistance) مناسبة للتطبيق في منظومات الخلايا الشمسية بمقدار (21.24 Ω / sq) بعد فترة الاختبار، أظهرت الدراسة أن التحكم في آلية ترسيب أفلام (AZO) من خلال تعديل متغيرات الترسيب كمسار فعال لتحسين الاستقرار البيئي للموصلية الكهربائية للأقطاب الكهربائية من أفلام (AZO) المصنعة عند درجات حرارة منخفضة.

Keywords: *JAZO electrodes, RF-sputtering, Electrical properties, IEC 61646 test, Environmental stability.*

1. INTRODUCTION

Transparent electrodes are ubiquitous in many optoelectronic applications including thin film solar cells and flat panel displays. For thin film solar cells, transparent electrodes are used to allow for solar radiation transmission to the cells' active layer, where photocurrent is generated, as well as for electrical current collection with minimum losses [1,2]. Due to the increasing interest and advancements in solar cells' technologies, wide range of materials are examined and applied as transparent electrodes [2,3]. Transparent conducting oxides (TCOs) have been an active research area since they combine high visible light transparency,

due to their wide-bandgap (Eg > 3 eV), with controllable electrical characteristics. For instance, indium tin oxide (ITO), tin-doped semiconductor, is the industry standard material for transparent electrodes' applications. However, the rapidly increasing demands for transparent electrodes coupled with the steadily increasing cost of ITO have stimulated research interests in ITO alternatives including, but not limited to, other oxide semiconductors, graphene, carbon nanotubes, and metal nanowire networks [3]. Among the most probable alternatives with widespread attention are zinc oxide based TCOs, such as aluminium doped zinc oxide (AZO) due to its resource availability and its relatively low cost [2,3]. ZnO-based transparent electrodes including AZO typically exhibit columnar microstructure of high grain boundary density where the trap states are localised and then strongly impede the carrier transport between neighbouring grains. Degenerate doping with various elements such as aluminium (Al) and gallium (Ga) is used to overcome the impact of grain boundaries on carries mobility of ZnO-based electrodes through increasing the free electron density. Hence, grain boundaries defects and the associated potential barrier are deactivated resulting in electrons tunnelling between adjacent grains. An enhancement in the Hall mobility is considered as an efficient strategy to enhance the electrical characteristics of TCOs with minimal effects on their optical characteristics [4,5]. Multiple reports of AZO transparent electrodes have been made with electrical and optical properties close to those of ITO electrodes and produced via various deposition techniques and post-deposition annealing techniques [6–10]. Despite of AZO merits, its electrical characteristics' stability against severe environmental conditions such as elevated temperature and humidity is still relatively low compared to that of ITO, which limits AZO electrodes' applications [11–14]. These environmental conditions are unavoidable when transparent electrodes are applied to potential long-life applications in harsh climatic environments such as solar cells. Upon environmental ageing, the evidenced conductivity degradation of ZnO-based transparent electrodes is attributed to adsorption of O_2 and H_2O defects from the test ambient into ZnO columnar microstructure [11–13]. These defects and their products such as hydroxides at grain boundaries and voids tend to trap electrons from the conduction band via charges recombination, i.e. free electron density (N) reduction, causing band bending and electrons depleted areas on both sides of grain boundaries. Consequently, the potential barriers height between neighbouring grains that free electrons have to overcome is increased leading to increasing electrons scattering at the grains boundaries, i.e. free electron mobility (μ) reduction [4,12,15]. For accelerated environmental ageing studies, the International Electrotechnical Commission (IEC) 61646 test is applied to examine lifetime stability and degradation rates of materials applied to solar cells' technologies. The test follows protocols that are designed to ensure a long-term warranty and it is estimated that the test represents about 20 years of field environment in Miami [2,16]. The test is implemented by subjecting solar cells' materials to a stressor in a controlled environment of damp heat conditions (temperature of 85°C and 85% relative humidity RH) during a period of 1000 h and monitoring the materials' essential characteristics [16]. The test conditions simulate failure modes observed in the field environment of solar cells and help to provide insights into the mechanisms involved in solar cells' materials degradation. Consequently, pathways for more durable materials are identified leading to better solar cell modules' lifetime stability. In the view of solar cells' technology, the environmental stability of transparent electrodes' electrical characteristics is directly linked to the solar cell modules' performance and efficiency stability. Increasing the electrodes' resistivity is a failure mode that results in increasing the solar cells series resistance and in decreasing the photo-generated current density [2,17]. Thus, for the developments of AZO transparent electrodes for solar cells with sustainable output power, the environmental stability of AZO electrical characteristics is being investigated under severe environmental conditions. Kim et al. [12] quantitatively studied the stability and degradation mechanisms of sputter-deposited AZO at 400°C and subsequently subjected to humid and hot environment for 800 h. The authors reported that the observed AZO resistivity increased by 64.70% (to 1.9×10^{-3} Ω.cm) upon the test is originated from the chemisorbed OH- defects at grain boundaries resulting in reducing both the electron density and mobility. Hüpkes et al. [13] demonstrated the effectiveness of high temperature annealing at 650°C in vacuum atmosphere for 24 h to fabricate very stable AZO electrodes compared to the as-deposited electrodes that exhibited a factor of 2-3 resistivity increase when exposed to DH test for 1000 h. Tabassum et al. [18] observed several cracks and voids for AZO transparent electrodes prepared by sol-gel technique, whereas no cracks were observed for sputter-deposited

AZO electrodes when exposed to harsh environment. Consequently, the sheet resistance of sol-gel prepared samples increased by >3000% (to 1800 Ω/sq) after 12 h, while the sputter-deposited samples sheet resistance increased by about 140% (to 67 Ω/sq) after 30 days. Tohsophon et al. [19] showed that the electrical properties of sputtered AZO electrodes could be restored via annealing at 250 °C in vacuum after being exposed to DH environment that caused resistivity increase by a factor of three after the first 300 h of the test period. Mickan et al. [20] reported enhanced electrical properties and ambient moisture (35% RH) durability for AZO electrodes deposited at high substrate temperature up to 600 °C. Mirletz et al. [21] showed that employing a protective capping layer of APTES (3-ami- nopropyltriethoxysilane) resulted in greatly reduced resistivity increase percentage for AZO electrodes from 250% to 60% upon DH exposure. Machda et al. [22] examined the effect of the crystal orientations on AZO damp heat stability, AZO samples with different crystal growth orientations (110) and (002) were fabricated via sputtering at various argon gas flow mixed with a fixed oxygen gas flow. A change of crystal growth orientation from (110) to (002) was reported at higher argon gas flow during deposition. Then, the samples were subjected to damp heat exposure for 25 days at 85°C with 85% relative humidity. The samples with the (002) crystal orientation were more stable in electrical conductivity than those samples with the (110) crystal orientation. Electrical conductivity degradation was mostly assigned to decreasing the carrier density for the (110) samples. Machda et al. [23] examined the DH stability of AZO thin films deposited at low temperature (80 °C) on glass and slide-glass and flexible polyimide-tape attached to polycarbonate (PI-tape/PC) substrates. Upon the DH exposure at 85 °C and 85% relative humidity for 25 days, AZO samples deposited on PI-tape/PC substrates exhibited noticeable sheet resistance by 600% (to 70 Ω/sq), this increase was mostly assigned to physical characteristics such as cracks caused by the test, rather than chemical characteristics, resulting in Hall mobility reduction. In contrast, AZO samples on glass substrates demonstrated no cracks as well as stable electrical properties. Theelen et al. [24] studied the degradation behaviour and mechanisms of oxide/metal/oxide (OMO) layer stacks deposited on glass via subsequent sputtering of AZO/sliver (Ag)/AZO. The silver layer significantly reduced the stacks sheet resistance from 540 ± 30 Ω/sq to 33 ± 3 Ω/sq. Following the exposure to damp heat (85 °C and 85% RH), however, complete loss of conductivity was observed after about 50 h of the test, this was attributed to the interaction between humidity, diffused through the grain boundaries of top AZO layer, and the intermediate silver layer causing migration and coalescence of the silver and thus breaking the silver layer into large islands. These islands then further coalesced creating thicker particles that would break through the top AZO layer creating large compressive stress and voids leading to conductivity loss. To separate effects of humidity and temperature, the authors examined also the samples' dry heat stability and no degradation was observed in the samples' conductivity under the absence of humidity. Low temperature fabrication is of paramount importance for top electrodes applied to thin film solar cells to avoid irreversible damage to the modules' active layer interfaces. In addition, Low temperature and less complicated fabrication routes of solar cells' materials are very essential for the realisation of low cost polymer-based solar cells [2,3,25]. To identify the physical characteristics controlling the adsorption of environmental defects into AZO and thus to identify pathways towards low temperature fabricated and environmentally stable AZO, this paper investigates the correlation between room temperature deposition conditions and environmental stability of AZO. Different deposition parameters are applied, without external heating during deposition nor any post processing annealing, to induce variations in the AZO physical characteristics, which would result in AZO films of different degradation rates.

2. EXPERIMENTAL PROCEDURE

2.1. AZO Transparent Electrodes' Deposition Procedure

AZO thin films were deposited on glass substrates at different deposition parameters and with no intentional substrate heating using radio frequency (RF) magnetron sputtering technique. The AZO thin films deposition procedure is fully reported previously [6]. Considering the as-deposited samples' conductivity, the optimised deposition parameters are an applied RF power of 180 W (on a sputtering target of 3" in diameter) and a sputtering pressure at 2 mTorr [6]

2.2. Transparent Electrodes' Environmental Stability Evaluation

Table 1. Presents the examined AZO and ITO transparent electrodes' details.

Samples set	Deposition details	Sheet resistance (Ω/sq)	Transparency at λ= 550 nm
AZO (1)	180 nm Thick at 180 W and 2 mTorr	50.83	83%
AZO (2)	180 nm Thick at 180 W and 5 mTorr	265.56	80%
AZO (3)	180 nm Thick at 120 W and 2 mTorr	89.44	82%
AZO (4)	360 nm Thick at 180 W and 2 mTorr	16.95	81%
ITO (Ref.)	150 nm Thick from Kintec Company	≈ 8	87%

The AZO samples listed in table 1 were subjected to the IEC 61646 qualification test. 150 nm thick high-quality ITO samples on glass substrates were also examined as reference samples for comparison with AZO. A THERMOTRON test chamber was used for the test, all the samples were not encapsulated and their area was (1 cm × 1 cm). A short run of the test was performed for ten days to examine the used chamber stability at the test conditions; it was found that the chamber maintains well the test conditions over long operating times demonstrating only ≈ 4% humidity changes during samples loading/unloading. For the IEC 61646 test, a batch of four AZO or ITO samples of the same fabrication conditions was used. A sample of each group was removed from the chamber every ten days of the test period (1000 h ~ 41days) for sheet resistance (R_{sh}) characterisation by a four-point probe (4PP) system to monitor the sheet resistance degradation. The sheet resistance degradation index denoted as (DI) was used to compare the examined transparent electrodes degradation rates. DI is calculated as the ratio between the samples' sheet resistance at the duration (x) of the IEC 61646 test (R_{Shx}) and the as-deposited samples' sheet resistance (R_{Sh0}) using the following equation:

$$DI = R_{Shx}/R_{Sh0} \quad \text{..... (1)}$$

The AZO films' thickness (t) was monitored during the deposition (via an online in situ interferometric monitor) and measured post deposition with a profilometer. Then, the corresponding samples resistivity (ρ) was determined from the 4PP measurements ($\rho = R_{sh}.t$). Also, all the samples had Hall Effect measurements pre and post the test to study the contributions of electrons density (N) and Hall mobility (μHall) into the samples' resistivity changes upon the test. Hall Effect measurements were performed using a Phystech RH2035 Hall measurement system operating in the Hall-Van der Pauw (VDP) configuration and equipped with a magnetic field of 0.54 T. It is worth mentioning that the 4PP and Hall Effect measurements were always performed at ambient conditions and consistent resistivity measurements were obtained from both techniques. Prior to the IEC 61646 test, the samples' ambient ageing (under ambient temperature and moisture) was monitored for 40 days via sheet resistance measurements every ten days. After the test, the sheet resistance for the examined samples was monitored under ambient conditions for 40 days to elucidate any possible sheet resistance changes that could be caused following the damp heat exposure. This robust examination (that includes the samples' performance for 40 days before the IEC 61646 test as well as for 40 days after the test) is rarely reported in literature. To investigate and explain the mechanisms involved in the AZO samples conductivity degradation, X-ray diffraction (XRD) and atomic force microscope (AFM) were used. High-resolution XRD patterns were collected using an X-Pert Panalytical diffractometer with Cu-Kα radiation (λ=1.5418 Å). The diffractometer was operated at 40 kV and 35 mA in Bragg–Brentano configuration. The collected XRD data was studied using Voigt-function analysis to extract the average grain size information from the XRD peak broadening, following the approach by De Keijser et al [26]. Scherrer's formula used to estimate the average grain size [27],

$$D = 0.94\lambda/\left(\tau_{Lorentzian} \times \cos\left(\frac{2\theta}{2}\right)\right) \quad \text{..... (2)}$$

where D is the average grain size in angstrom, λ is the X-ray wavelength, $\tau_{Lorentzian}$ is the integral breath of the Lorentzian component of the XRD peak, associated with grain caused broadening, and 2θ is the Bragg angle in radians.

The integral breath (τLorentzian) is reported to result in more accurate estimation of the average grain size than using the full width at half maximum (FWHM) of the XRD peak Lorentzian component (βLorentzian). τLorentzian and βLorentzian are related by the following equation [28]

$$\tau_{Lorentzian} = \beta_{Lorentzian} \times \frac{\pi}{2} \quad \text{..... (3)}$$

AFM surface morphology features were examined using a Digital Instruments Nanoscope IV Dimension 3100 scanning probe microscope operated in tapping mode. ITO electrodes' microstructure and morphological characteristics were not studied in this work and the comparison between AZO and ITO electrodes was based only on the electrical characteristics' measurements.

3. RESULTS AND DISCUSSION

Under ambient temperature and moisture, the examined transparent electrodes demonstrated high stability with almost no sheet resistance changes for a period of 40 days. However, under the IEC 61646 test conditions, the samples' sheet resistance increased linearly over the test period, demonstrating different degradation rates. The averaged 4PP measurements presented in figure 1 (a) illustrate that the AZO samples' damp heat (DH) stability is directly linked to the deposition conditions applied. The AZO (2) set of samples deposited at relatively high sputtering pressure, 5 mTorr, exhibited a substantial sheet resistance increase of about 136.40% and a degradation index of 2.36 for the IEC 61646 test period. Moreover, the sheet resistance of these samples continued to rise even after the test period demonstrating a total of 230.54% increase and 3.30 degradation index in a period of 40 days after the test. Reducing the sputtering pressure to 2 mTorr, AZO (1) samples, was found to noticeably enhance the AZO samples DH stability resulting in 49.72% sheet resistance increase and 1.49 degradation index. Also, the sheet resistance of these samples exhibited much less pronounced changes during the 40 days after the test period, relative to the higher pressure AZO (2) samples, with a total increase of 56.28% and a degradation index of 1.56, as shown in figure 1.

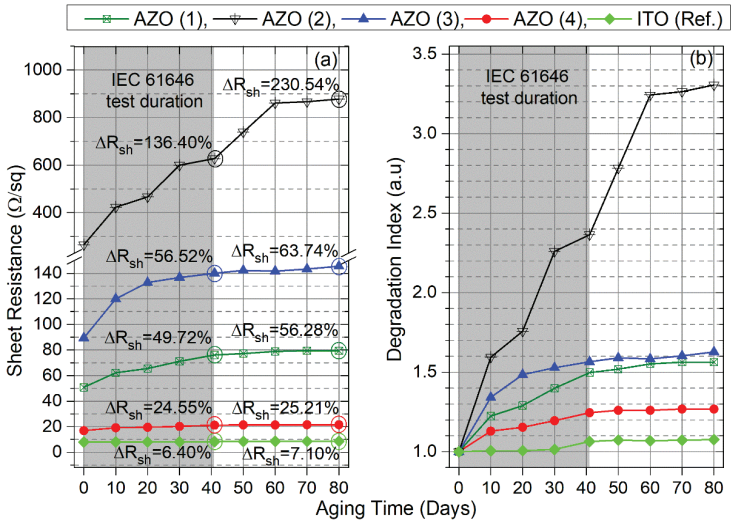

Figure (1). The examined transparent electrodes' averaged sheet resistance measurements (a) and degradation index (b) versus the aging time. Grey areas correspond to the IEC 61646 test duration, (the lines are an aid to the eye).

The correlation between the AZO samples' deposition parameters and the samples' DH stability was also revealed by the AZO (3) set of samples deposited at 2 mTorr and 120 W, demonstrating 56.52 % sheet resistance increase and 1.56 degradation index for the test period. The AZO (3) samples' DH stability upon the test was marginally worse compared to that for AZO (1) deposited at 2 mTorr and 180 W (49.72 % Rsh increase and 1.49 DI), but noticeably much better relative to that for AZO (2) samples deposited at 5 mTorr and 180 W (136.40 % Rsh increase and 2.36 DI). From figure 1, it is also clear that increasing the AZO samples thickness from 180 nm to 360 nm at 180 W and 2 mTorr noticeably improves the AZO (4) samples' DH stability compared to AZO (1) samples. The 360 nm-thick samples maintained low sheet resistance values of about 21.24 Ω/sq even after the test conditions exposure, demonstrating just 24.55% sheet resistance increase and 1.24 degradation index for the test period. Considering the reference samples of ITO, an excellent DH stability was observed for the test period (DI=1.06) as well as for the 40 days after the test under ambient condition (DI=1.07)

The XRD spectra for the examined AZO samples collected in a wide range of 2θ angles (30° to 80°) showed two crystalline peaks at 2θ values of 34.39°± 0.02° and 72.50°± 0.02° (figure 2 inset (a)), corresponding to the hexagonal wurtzite structure (002) and (004) planes of ZnO, respectively.

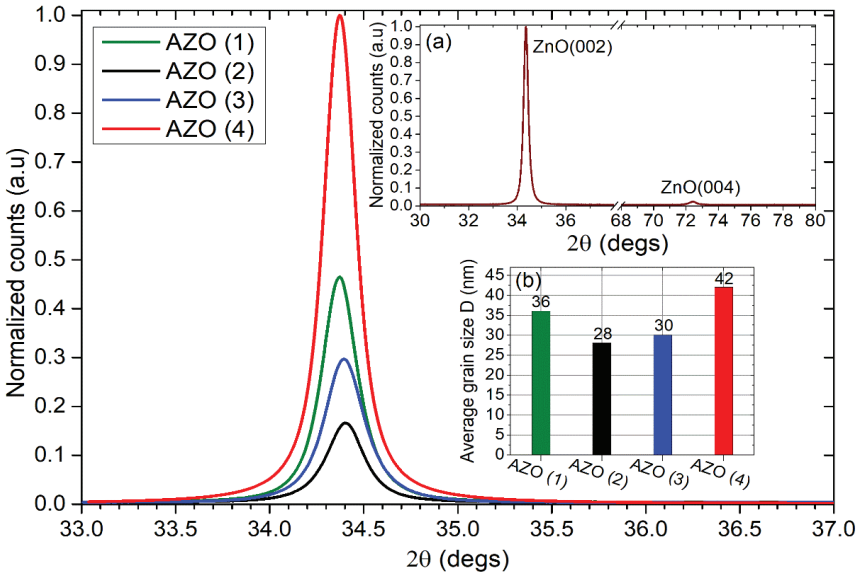

Figure (2). Normalized XRD patterns for the examined AZO transparent electrodes pre the IEC 61646 test. Inset (a) shows a normalized wide XRD pattern for the AZO (1) set of samples. Inset (b) presents the average grain size for AZO transparent electrodes obtained from Voigt-function analysis applied to the ZnO (002).

XRD analysis using Voigt-function applied to the ZnO (002) diffraction peak for the collected XRD patterns revealed that increasing the sputtering pressure from 2 mTorr to 5 mTorr results in average grain size reduction from ≈ 36 nm to ≈ 28 nm for AZO (1) and AZO (2) sets of samples, respectively, as shown in figure 2 inset (b). Smaller grain size implies a lower columnar microstructure compactness, a smaller distance between microstructural defects allocated perpendicular to the substrate surface, and a larger volume of grain boundary and other lattice defects for AZO (2) samples. Moreover, the XRD pattern for the AZO (2) set of samples illustrated a lower ZnO (002) intensity and a larger full width at half maximum FWHM (0.24 deg) relative to (0.22 deg) for the AZO (1) set of samples which would be attributed to a lower degree of grains alignment (i.e. crystallinity) [17,29]. These findings conclude that AZO (2) samples, deposited at 5 mTorr, contain a higher amount of crystalline imperfections compared to AZO (1) samples, deposited at 2 mTorr. In

contrast, increasing the AZO samples thickness to 360 nm for the AZO (4) set of samples caused a higher ZnO (002) intensity and smaller FWHM (0.20 deg) indicating enhanced crystallinity. Voigt-function analysis, figure 2 inset (b), demonstrated that the 360 nm thick AZO (4) samples have an average grain size of ≈ 42 nm compared to ≈ 36 nm for AZO (1) samples of 180 nm thickness implying reduced grain boundaries density and defects within the grains [29]. It should be highlighted that the XRD patterns for all the AZO samples exposed to the test conditions do not reveal clear evidence for crystal structure changes induced by the test conditions. This result agrees with the findings of [11,12,15] and implies that the sheet resistance degradation is associated with the adsorbed defects at the non-crystalline regions (i.e. grain boundaries).

AFM images presented in figure 3 (a and b) showed that increasing the sputtering pressure to 5 mTorr for AZO (2) samples results in noticeable surface profile changes with more separation voids in between which revels less compactness compared to AZO (1) samples of 2 mTorr. The images also showed an increase in the surface roughness at higher sputtering pressure, the Root Mean Square roughness (R_{RMS}) increased from 1.72 nm for AZO (1) samples to 2.52 nm for AZO (2) samples. After Igasaki and Kanma [30], larger surface roughness reveals larger effective surface area for the AZO (2) samples. This is indicated by the noticed increase in the mean roughness depth (Zrange) from 12.40 nm for AZO (1) samples to 20.30 nm for AZO (2) samples.

The XRD and AFM findings for AZO (1) and AZO (2) samples are well explained by the Structure Zone Model (SZM) developed by Thornton to correlate the microstructure and morphology properties of sputtered films with both the substrate temperature and the sputtering pressure [31]. Based on the SZM, higher sputtering pressure alters the microstructure and morphological characteristics of the resulting films from densely packed grains to tapered grains with much pronounced separation voids. This is attributed to intensified collisions between the sputtered species and the background sputtering gas ions at higher sputtering pressure resulting in reducing the species kinetic energy which in turn limits the species surface diffusion and growth dynamics producing defective AZO films. The above observed crystalline and morphological imperfections for the AZO (2) set of samples are considered as possible pathways for environmental defects adsorption from the test ambient into AZO samples [11,19]. Hence, these imperfections of AZO (2) samples would facilitate the adsorption and reaction of higher density of O_2 and H_2O defects under the IEC 61646 test conditions [11,12,32]. The adsorbed defects and their products continued to drastically deteriorate the sheet resistance for the AZO (2) set of samples even after the test period as shown in figure 1. This would indicate higher density of adsorbed defects for the AZO (2) set of samples compared to the other examined AZO samples. The roughness details for AZO (2) samples deposited at (180 W and 5 mTorr) and AZO (3) samples deposited at (120 W and 2 mTorr) shown in figure 3 (b and c) could explain the noticed difference in the degradation indexes for these samples (2.36 vs. 1.56, as presented in figure (1-b)) despite having very close average grain sizes (≈ 28 nm and ≈ 30 nm as shown in the inset (b) of figure 2). In other words, the different aging rates for these two sets of samples would be assigned to the morphological characteristics of the AZO (2) set of samples. Both the applied RF power and the sputtering pressure influence AZO environmental stability through different growth dynamics. However, the sputtering pressure was found to have the most pronounced effects on the growth process of AZO samples with the effects being directly linked to AZO samples crystalline and morphological characteristics and compactness. Therefore, optimising the AZO deposition parameters enhances the AZO samples' microstructure and morphological characteristics as well as densification leading to enhanced DH stability.

Hall Effect measurements presented in figure 4 confirmed that the AZO electrodes' conductivity durability upon the IEC61646 test is directly linked to the applied growth conditions. For instance, AZO (2) samples deposited at 5 mTorr were the most sensitive samples to heat and humidity, exhibiting conductivity worsening ratio that is about two times larger than that for AZO (1) samples deposited at 2 mTorr.

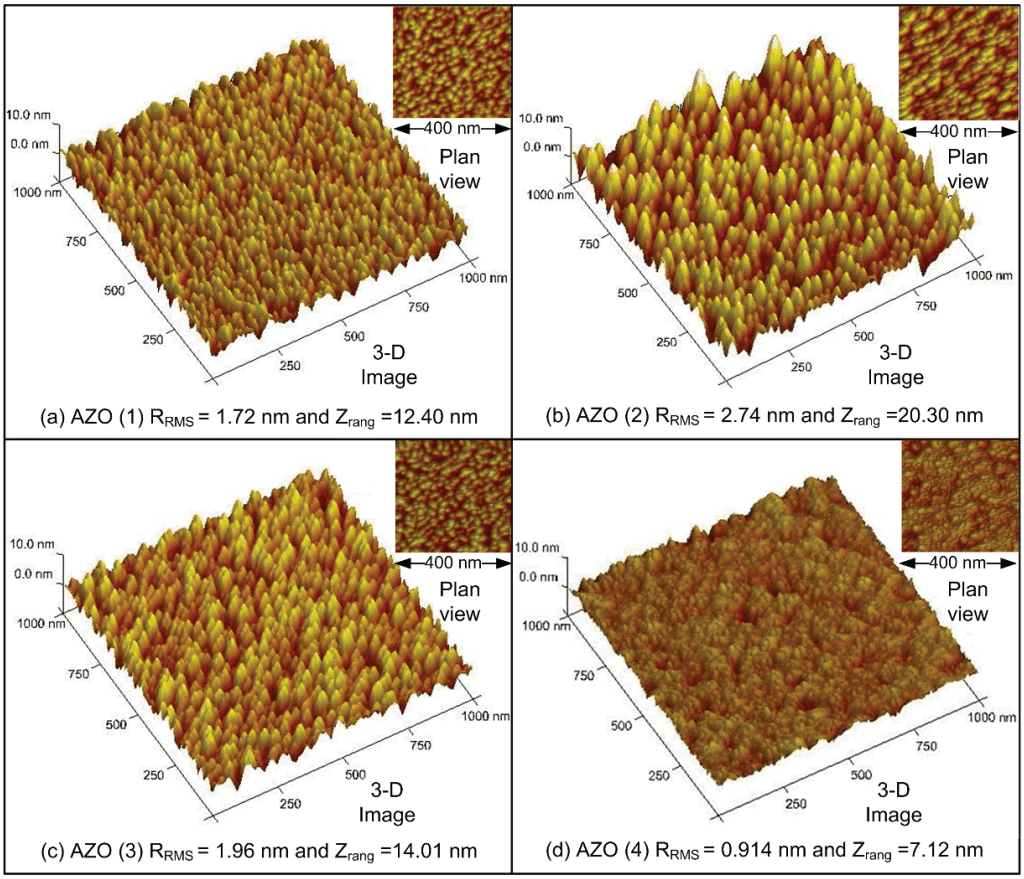

Figure (3). AFM images (3D and Plan view) and roughness details for the AZO transparent electrodes pre the IEC 61646 test.

A close look at the Hall Effect data illustrates that the resistivity increase for AZO (1) samples post the test is more associated with the Hall mobility (μ_{Hall}) reduction by 19% relative to 13% drop in the free electron density as shown in figure 4. This would be attributed to increased electron depleted areas within grains, potential barriers between grains, and thus increased grain boundaries scattering, caused by the adsorbed defects [5,12,33]. However, the resistivity of AZO (2) samples deposited at 5 mTorr increased upon the test due to the free electron density reduction by about 59% relative to 26% decrease in the Hall mobility. The behaviour of AZO (2) samples could be linked to a lager density of adsorbed defects from the test ambient via the observed larger amount of microstructure and morphological imperfections for these samples compared to AZO (1) samples. Hence, to deactivate the adsorbed defects at the imperfections of AZO (2) samples, higher density of free electrons is trapped from the grains and immobilised relative to AZO (1) samples. Also, due to a smaller density of free electrons of $2.12\times10^{20}/cm^3$ for AZO (2) samples compared to $3.84\times10^{20}/cm^3$ for AZO (1) samples, the electron density for the former is reduced due to the IEC 61646 test by 59% compared to 13% for the latter. Therefore, wider carrier-depleted areas and higher potential barriers between adjacent grains are created within AZO (2) samples. Consequently, the Hall mobility for AZO (2) samples is reduced by 26% relative to 19% for AZO (1) samples. As for the 360 nm thick and most stable AZO samples in this work, figure 4 revealed that the electron density and Hall mobility of AZO (4) samples were reduced by 10% and 13% respectively, compared to 13% and 19% for the 180 nm thick samples of AZO (1)

set. The enhanced DH stability for AZO (4) samples is attributed to the microstructure and morphological characteristics of these samples as observed via AFM images and XRD data. Doubling the thickness at the same deposition conditions for AZO (4) samples resulted in reducing considerably the roughness R_{RMS} to 0.914 nm and enhancing the grain size to ≈ 42 nm compared to roughness R_{RMS} of 1.72 nm and a grain size of ≈ 36 nm for AZO (1) samples. These results indicate less pronounced grain boundaries and more compact structure for thicker AZO samples [32]. Hence, thicker AZO samples have the advantage to hinder the in-diffusion of conductivity detrimental defects (O_2 and H_2O) leading to the electrical characteristics of these samples being influenced less by the DH exposure. It is reported that ITO presents a barrier to adsorbed defects by means of these defects accumulating on the surface of ITO samples instead of diffusing into the bulk [34]. Also, ITO films exhibit a lower density of grain boundary traps compared to ZnO-based films [4,15]. These characteristics contribute to enhanced DH stability for ITO films' electrical properties. Figure 4 shows just below 7% resistivity increase for ITO that is originated mainly from the carrier density reduction upon the test. As far as the visible transmittance (at λ= 550 nm) is considered, the examined transparent electrodes demonstrated very limited changes following the test exposure.

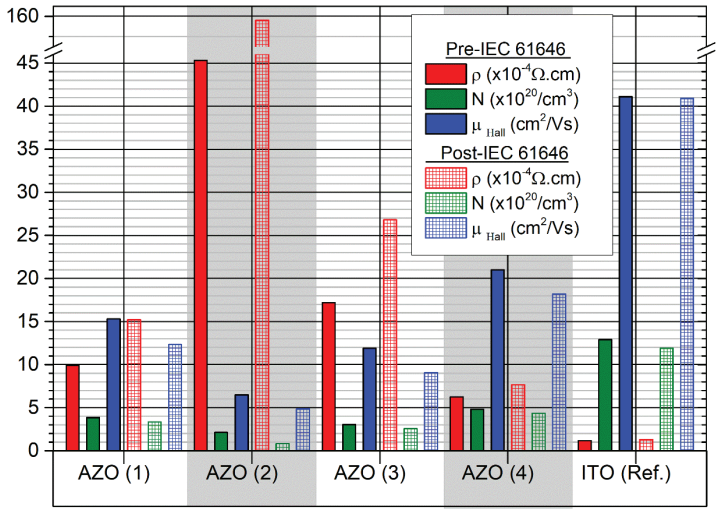

Figure (4). Averaged data of resistivity (ρ), carrier density (N), and Hall mobility (μ_{Hall}) for the examined transparent electrodes pre the IEC 61646 test (solid bars) and post the IEC 61646 test (dashed bars).

4. CONCLUSION

The environmental stability of AZO electrodes' electrical properties was investigated under the IEC 61646 qualification standard to evaluate their failure modes when applied to solar cells. The adsorption of O_2 and H_2O defects (AZO conductivity failure causes) from the test environment to AZO structure is increased at larger density of microstructure and morphological imperfections. Hence, AZO electrical properties are degraded at faster and more noticeable rates. Optimising the growth dynamics though exploring different deposition conditions resulted in enhanced physical characteristics and thus enhanced environmental stability for low temperature deposited AZO electrodes. Upon the test, a resistivity increase of 24.55 % (to 7.64×10-4 Ω.cm, corresponding to a sheet resistance of 21.24 Ω/sq) was observed for the most stable AZO electrodes in this work, deposited at the optimised conditions, compared to 6.40% for ITO as the industrial standard transparent electrode material. These electrodes, therefore, could be employed in thin film solar cells which require environmentally stable and low temperature fabricated front electrodes. AZO electrodes deposited at the non-optimised conditions were more affected by the test conditions during the test period as well as during 40 days after the test.

REFERENCES

[1]. M.A. Green, Thin-film solar cells: Review of materials, technologies and commercial status, in: J. Mater. Sci. Mater. Electron., 2007. https://doi.org/10.1007/s10854-007-9177-9.

[2]. Transparent conductive zinc oxide: basics and applications in thin film solar cells, Choice Rev. Online. 45 (2008). https://doi.org/10.5860/choice.45-6197.

[3]. K. Ellmer, Past achievements and future challenges in the development of optically transparent electrodes, Nat. Photonics. 6 (2012). https://doi.org/10.1038/nphoton.2012.282.

[4]. K. Ellmer, Resistivity of polycrystalline zinc oxide films: Current status and physical limit, J. Phys. D. Appl. Phys. 34 (2001). https://doi.org/10.1088/0022-3727/34/21/301.

[5]. T. Minami, H. Sato, K. Ohashi, T. Tomofuji, S. Takata, Conduction mechanism of highly conductive and transparent zinc oxide thin films prepared by magnetron sputtering, J. Cryst. Growth. 117 (1992). https://doi.org/10.1016/0022-0248(92)90778-H.

[6]. S.O. El Hamali, W.M. Cranton, N. Kalfagiannis, X. Hou, R. Ranson, D.C. Koutsogeorgis, Enhanced electrical and optical properties of room temperature deposited Aluminium doped Zinc Oxide (AZO) thin films by excimer laser annealing, Opt. Lasers Eng. 80 (2016). https://doi.org/10.1016/j.optlaseng.2015.12.010.

[7]. D. Scorticati, A. Illiberi, T.C. Bor, S.W.H. Eijt, H. Schut, G.R.B.E. Römer, M. Klein Gunnewiek, A.T.M. Lenferink, B.J. Kniknie, R. Mary Joy, M.S. Dorenkamper, D.F. De Lange, C. Otto, D. Borsa, W.J. Soppe, A.J. Huis In 't Veld, Thermal annealing using ultra-short laser pulses to improve the electrical properties of Al:ZnO thin films, Acta Mater. 98 (2015). https://doi.org/10.1016/j.actamat.2015.07.047.

[8]. Q. Nian, M.Y. Zhang, B.D. Schwartz, G.J. Cheng, Ultraviolet laser crystallized ZnO:Al films on sapphire with high Hall mobility for simultaneous enhancement of conductivity and transparency, Appl. Phys. Lett. 104 (2014). https://doi.org/10.1063/1.4879643.

[9]. B. Ayachi, T. Aviles, J.P. Vilcot, C. Sion, Rapid thermal annealing effect on the spatial resistivity distribution of AZO thin films deposited by pulsed-direct-current sputtering for solar cells applications, Appl. Surf. Sci. 366 (2016). https://doi.org/10.1016/j.apsusc.2016.01.054.

[10]. S. Tabassum, E. Yamasue, H. Okumura, K.N. Ishihara, Electrical stability of Al-doped ZnO transparent electrode prepared by sol-gel method, Appl. Surf. Sci. 377 (2016). https://doi.org/10.1016/j.apsusc.2016.03.133.

[11]. M. Theelen, T. Boumans, F. Stegeman, F. Colberts, A. Illiberi, J. Van Berkum, N. Barreau, Z. Vroon, M. Zeman, Physical and chemical degradation behavior of sputtered aluminum doped zinc oxide layers for Cu(In,Ga)Se2 solar cells, Thin Solid Films. 550 (2014). https://doi.org/10.1016/j.tsf.2013.10.149.

[12]. J.I. Kim, W. Lee, T. Hwang, J. Kim, S.Y. Lee, S. Kang, H. Choi, S. Hong, H.H. Park, T. Moon, B. Park, Quantitative analyses of damp-heat-induced degradation in transparent conducting oxides, Sol. Energy Mater. Sol. Cells. 122 (2014). https://doi.org/10.1016/j.solmat.2013.12.014.

[13]. J. Hüpkes, J.I. Owen, M. Wimmer, F. Ruske, D. Greiner, R. Klenk, U. Zastrow, J. Hotovy, Damp heat stable doped zinc oxide films, Thin Solid Films. 555 (2014). https://doi.org/10.1016/j.tsf.2013.08.011.

[14]. F.J. Pern, R. Noufi, B. To, C. DeHart, X. Li, S.H. Glick, Degradation of ZnO-based window layers for thin-film CIGS by accelerated stress exposures, in: Reliab. Photovolt. Cells, Modul. Components, Syst., 2008: p. 70480P. https://doi.org/10.1117/12.795097.

[15]. J.H. Kim, H. Lee, S. Choi, K.H. Bae, J.Y. Park, Impact of water corrosion on nanoscale conductance on aluminum doped zinc oxide, in: Thin Solid Films, 2013. https://doi.org/10.1016/j.tsf.2013.03.100.

[16]. C.R. Osterwald, T.J. McMahon, History of accelerated and qualification testing of terrestrial photovoltaic modules: A literature review, Prog. Photovoltaics Res. Appl. 17 (2009). https://doi.org/10.1002/pip.861.

[17]. M. Hála, H. Kato, M. Algasinger, Y. Inoue, G. Rey, F. Werner, C. Schubbert, T. Dalibor, S. Siebentritt, Improved environmental stability of highly conductive nominally undoped ZnO layers suitable for n-type windows in thin film solar cells, Sol. Energy Mater. Sol. Cells. 161 (2017). https://doi.org/10.1016/j.solmat.2016.11.015.

[18]. S. Tabassum, E. Yamasue, H. Okumura, K.N. Ishihara, Sol–gel and rf sputtered AZO thin films: Analysis of oxidation kinetics in harsh environment, J. Mater. Sci. Mater. Electron. 25 (2014). https://doi.org/10.1007/s10854-014-2248-9.

[19]. T. Tohsophon, J. Hüpkes, S. Calnan, W. Reetz, B. Rech, W. Beyer, N. Sirikulrat, Damp heat stability and annealing behavior of aluminum doped zinc oxide films prepared by magnetron sputtering, Thin Solid Films. 511–512 (2006).

https://doi.org/10.1016/j.tsf.2005.12.130.

[20]. M. Mickan, U. Helmersson, D. Horwat, Effect of substrate temperature on the deposition of Al-doped ZnO thin films using high power impulse magnetron sputtering, Surf. Coatings Technol. 347 (2018). https://doi.org/10.1016/j.surfcoat.2018.04.089.

[21]. H.M. Mirletz, K.A. Peterson, I.T. Martin, R.H. French, Degradation of transparent conductive oxides: Interfacial engineering and mechanistic insights, Sol. Energy Mater. Sol. Cells. 143 (2015). https://doi.org/10.1016/j.solmat.2015.07.030.

[22]. F. Machda, T. Ogawa, H. Okumura, K.N. Ishihara, Damp Heat Durability of Al-Doped ZnO Transparent Electrodes with Different Crystal Growth Orientations, ECS J. Solid State Sci. Technol. 8 (2019). https://doi.org/10.1149/2.0261912jss.

[23]. F. Machda, T. Ogawa, H. Okumura, K.N. Ishihara, Damp-heat durability comparison of Al-doped ZnO transparent electrodes deposited at low temperatures on glass and PI-tape/PC substrates, Ceram. Int. 46 (2020). https://doi.org/10.1016/j.ceramint.2020.03.173.

[24]. M. Theelen, C. Hagedoorn, M. Götz-Köhler, A. Weeber, N. Neugebohrn, Damp heat induced degradation mechanisms occurring in coloured oxide/metal/oxide films for thin-film solar cells, Thin Solid Films. 730 (2021). https://doi.org/10.1016/j.tsf.2021.138711.

[25]. M. Wang, X. Hou, J. Liu, K.L. Choy, P. Gibson, E. Salem, D. Koutsogeorgis, W. Cranton, An alternative non-vacuum and low cost ESAVD method for the deposition of Cu(In,Ga)Se2 absorber layers, Phys. Status Solidi Appl. Mater. Sci. 212 (2015). https://doi.org/10.1002/pssa.201431295.

[26]. T.H. de Keijser, J.I. Langford, E.J. Mittemeijer, A.B.P. Vogels, Use of the Voigt function in a single-line method for the analysis of X-ray diffraction line broadening, J. Appl. Crystallogr. 15 (1982). https://doi.org/10.1107/s0021889882012035.

[27]. U. Holzwarth, N. Gibson, The Scherrer equation versus the "Debye-Scherrer equation," Nat. Nanotechnol. 6 (2011). https://doi.org/10.1038/nnano.2011.145.

[28]. A.R. Stokes, A.J.C. Wilson, The diffraction of x rays by distorted crystal aggregates - I, Proc. Phys. Soc. 56 (1944). https://doi.org/10.1088/0959-5309/56/3/303.

[29]. W. Water, S.Y. Chu, Physical and structural properties of ZnO sputtered films, Mater. Lett. 55 (2002). https://doi.org/10.1016/S0167-577X(01)00621-8.

[30]. Y. Igasaki, H. Kanma, Argon gas pressure dependence of the properties of transparent conducting ZnO:Al films deposited on glass substrates, Appl. Surf. Sci. 169–170 (2001). https://doi.org/10.1016/S0169-4332(00)00748-0.

[31]. J.A. Thornton, INFLUENCE OF APPARATUS GEOMETRY AND DEPOSITION CONDITIONS ON THE STRUCTURE AND TOPOGRAPHY OF THICK SPUTTERED COATINGS., in: J Vac Sci Technol, 1974. https://doi.org/10.1116/1.1312732.

[32]. W. Lin, R.X. Ma, J. Xue, B. Kang, RF magnetron sputtered ZnO:Al thin films on glass substrates: A study of damp heat stability on their optical and electrical properties, Sol. Energy Mater. Sol. Cells. 91 (2007). https://doi.org/10.1016/j.solmat.2007.07.008.

[33]. K. Ellmer, R. Mientus, Carrier transport in polycrystalline transparent conductive oxides: A comparative study of zinc oxide and indium oxide, Thin Solid Films. 516 (2008). https://doi.org/10.1016/j.tsf.2007.05.084.

[34]. T. Tohsophon, A. Dabirian, S. De Wolf, M. Morales-Masis, C. Ballif, Environmental stability of high-mobility indium-oxide based transparent electrodes, APL Mater. 3 (2015). https://doi.org/10.1063/1.4935125.